

Approximate Stochastic Self-Similarity of Envelopes of High-Frequency Teleseismic P -Waves from Large Earthquakes

ALEXANDER A. GUSEV^{1,2}

Abstract—A wavetrain of high-frequency (HF) P waves from a large earthquake, when recorded at a distant station, looks like a segment of modulated noise, with its duration close to the duration of rupture. These wavetrains, with their bursts and fadings, look much more intermittent than a segment of common stationary random noise. We try to describe quantitatively this bursty behavior. To this end, variogram and spectral analyses are applied to time histories of P -wave envelopes (squared-amplitude or instant-power signals) in six HF bands of 1-Hz width. Nine $M_w = 7.6$ – 9.2 earthquakes were examined, using, in total, 232 records and 992 single-band traces. Variograms of integrated instant power are approximately linear on a log–log scale, indicating that the correlation structure of the instant-power signal is approximately self-similar. Also, estimates of the power spectrum of the instant-power signal look approximately linear on a log–log scale. Log–log slopes of the variograms and spectra deliver estimates of the Hurst exponent H that are mostly in the range 0.6–0.9, markedly above the value $H = 0.5$ of uncorrelated (white-noise) signals. The preferred estimate over the entire data set is $H = 0.83$, still, this estimate may include some bias, and must be treated as preliminary. The inter-event scatter of H estimates is about 0.04, reflecting individual event-to-event variations of H . Many of the average log–log spectral plots show slight concavity that perturbs the approximately linear slope; this is a secondary effect that seems to be mostly related to the limited bandwidth of the data. Evidence is given in support of the idea that the observed approximately self-similar correlation structure of the P -wave envelope originates in a similar structure of the body wave instant-power signal radiated by the source, so that the propagation-related distortions can be regarded as limited. The facts presented suggest that the space–time organization of the earthquake rupture process is multiscaled and bears significant fractal features; it deviates from the brittle-crack model with its two well-separated characteristic scales. Phenomenologically, the high-frequency body-wave radiation from an earthquake source can be thought of as a product of stationary noise and the square root of a positive random envelope function with a power-law spectrum. From the viewpoint of applications,

the self-similarity of body wave envelopes provides a useful constraint for earthquake source models used to simulate strong ground motions.

Key words: Body wave, large earthquake, self-similar, variogram, power law, power spectrum, instant power, high frequency.

1. Introduction

The object of this study is the properties of teleseismic P -waves of large earthquakes, when considered in the high-frequency (HF) range i.e., at frequencies significantly above source corner frequency (in practice, above 0.3–0.5 Hz). These properties are interesting in themselves, and may bear important information regarding the properties of an earthquake rupture. In studies of HF body waves from large earthquakes, much interest has been directed at analysis of their duration and its relationship with magnitude. TRIFUNAC and BRADY (1975) noted that the duration of an accelerogram (i.e., HF signal) has a magnitude-related component. IZUTANI and HIRASAWA (1987) noted that this magnitude dependence can be used for rapid determination of the tsunami potential of an earthquake. In the seventies, the issue of teleseismic P -wave duration was the key point in the famous discrepancy between m_b versus M_s relationships determined by USA and USSR seismic networks. This controversy was resolved when it was found that the USA network before 1980 used only the first 6–9 s of a record to measure peak amplitude, resulting in saturation of m_b at moderate-to-large values of M_s or M_w , whereas the USSR network used actual, even, when needed, very late maxima, and did not feel true, “hard” saturation, only the decrease of the slope of the trend.

¹ Institute of Volcanology and Seismology, Russian Ac. Sci. 9 Piip Blvd, Petropavlovsk-Kamchatsky 683006, Russia. E-mail: gusev@emsd.iks.ru

² Kamchatka Branch, Geophysical Service, Russian Ac. Sci. 9 Piip Blvd, Petropavlovsk-Kamchatsky 683006, Russia.

This problem was elucidated by HOUSTON and KANAMORI (1986) who showed unequivocally the lack of “hard” saturation for full-record m_b of the greatest earthquakes, and gave the approximate relationships of HF teleseismic duration parameters versus magnitude.

A still unexplored characteristic of HF body waves is the correlation structure of their envelopes. Speaking of “envelope” here and below, we mean the time function that describes the behavior of instant variance or mean-square amplitude of the signal, and not the current value of the modulus of analytical signal. The correlation function of an HF signal itself is not very informative, resembling that of band-limited white noise. A much more promising subject is the correlation structure of the time function of instant HF power. Envelopes of short-period teleseismic records of P -waves of large earthquakes look intermittent and bursty, and one can hypothesize that they have self-similar, or fractal, structure (MANDELBROT, 1982). This idea is tested in the following text.

There are two standard approaches to study the correlation structure of apparently random observed functions: to construct a variogram (delta-variance) in the time domain or to estimate the power spectral density (PSD) in the frequency domain (MANDELBROT, 1982). In the case of self-similarity, both these functions must be power laws. Both methods of analysis must produce compatible estimates of the Hurst exponent, H , that is the main single parameter that describes a self-similar signal. For self-similar, positively correlated fractal signals H must be in the range $H = 0.5-1$. For a variogram, its slope on a log-log scale is merely $2H$. PSD behaves as $1/f^\alpha$, where the exponent $\alpha = 2H - 1$ is in the range $0-1$. When α is close to unity, such signals are called flicker-noises (“pink noises”). Our intention is to show that positive flicker noise may be a reasonable representation of a signal of instant power (or squared amplitude) of an HF body wave train from a large earthquake.

The concept of self-similarity of signals and functions has been proposed previously in earthquake seismology, but along different lines. HASKELL (1966) and AKI (1967) introduced earthquake spectral models with power-law high-frequency tails. ANDREWS (1980, 1981) noted that this behavior can be related to

power-law shapes of HF frequency and wavenumber spectra (and thus, to stochastic self-similarity or fractal behavior) for such functions as source slip rate, stress drop and final slip. In the framework of Andrews’ approach, however, the self-similarity is manifested as power-law spectra of these functions proper, and not of their envelopes. The stochastic temporal structure of signal envelopes was not considered by Andrews; in his illustration he uses a slowly varying deterministic envelope function with its duration near the to inverse corner frequency. Along a similar line, the strong-motion acceleration signal was modeled as a segment of band-limited white (HANKS and MCGUIRE, 1981; BOORE, 1983) or colored (GUSEV, 1983) noise, extracted from an infinite stationary signal by using boxcar or another simple-shaped *deterministic* window. Such window or modulating function is, in essence, the square root of the time-dependent mean (ensemble-average) instant power. Neither stochastic nor non-trivial (e.g., hierarchal) deterministic structure is present in modulating functions used in these models. The representation considered here is conceptually different: it assumes that the modulating function is *random*.

A number of studies of stochastic self-similar temporal structures have been performed in seismology, but they mostly were aimed at earthquake catalogs. These are known to consist of scale-invariant clusters, with the Omori law as an evident prototype. The fractal structure of earthquake catalogs proper was first shown by RYKUNOV *et al.*, (1987) for large earthquakes, small earthquakes, micro-earthquakes, and also for microseismic signals of endogenic origin (“seismic emission”) treated as a sequence of pulses. Self-similarity of seismological time functions was revealed by URQUIZU and CORREIG (1998), for common microseisms and S coda.

Generally, the HF time function of an earthquake reflects the history of source formation. However, multipathing and scattering along the ray introduce distortion of the source signal. KOPNICHV (1977) noted that the envelope of the squared band-filtered teleseismic record may be approximately represented as convolution of source and path contributions. We shall call the path-related contribution the “instant power Green function” or IPGF. The convolution

representation clarifies why only large, long-source-duration earthquakes show clear the source-related pattern of envelopes. Moreover, one can consider a squared envelope of a small, short-source-duration earthquake as an empirical estimate of the IPGF (shortened to “EGF”). Generally, the P wave IPGF consists of two main components: the combination of P , pP , sP and secondary phases, with individual spikes often unidentifiable, and total duration typically no more than 10 s, and a long relatively smoothly decaying coda of limited amplitude. The possibility of considering EGF as a proxy for IPGF has two consequences. First, note that a squared HF signal of an $M \approx 5$ earthquake, taken as EGF, has the structure as described above, with limited duration of the main peak. Therefore, the main features of HF time functions of earthquakes with rupture duration in excess of 20 s (or, roughly, $M > 7.3$) will be distorted only to a limited degree. Second, one can approximately deconvolve the source-related time function, using EGF to construct the inversion operator. The first attempt of this kind was that of KOPNICHEV (1977). This approach was developed more systematically by GUSEV and PAVLOV (1991) (see also GUSEV *et al.*, 2007) who successfully determined temporal centroids and durations of source HF envelopes radiated to many stations/rays, and from these data, using the Doppler effect, were able to recover source durations and rupture termination points, and the space–time HF energy centroids of a source.

The contamination of the source signal by multipathing and P coda formation dictates caution when one tries to deduce the correlation properties of fault radiation from similar properties of the observed teleseismic P -wave train. It can be noted, however, that during convolution, the spike-like components of IPGF (P , pP , sP) that are the most powerful (they contain no less than half the total energy) cannot create a systematic self-similarity pattern in principle. The distorting effect of coda cannot be excluded a priori. We shall try to show experimentally, in two ways, that at frequencies below 1/10 s, the combined distortion related to the IPGF cannot be significant. First, we shall show that EGFs, when analyzed by our technique, do not show a clear self-similarity imprint, and thus can hardly impose it on to the observed

teleseismic signal. Second, we shall analyze a few deconvolved envelopes, and show that the self-similarity pattern, where observable, is preserved after deconvolution.

There are significant technical limits that impede the data analysis aimed at revealing the stochastic structure of HF P -wave envelopes. Ideally, in order to increase the reliability of results and to improve the accuracy of numerical estimates, one would use signal durations as long as possible and signal bandwidths as wide as possible. In reality, the duration of a rupture puts a natural upper limit to the length of the data window. As for the usable signal bandwidth, it is strictly limited (at the HF side) by P -wave attenuation along the ray path. As a result, even with relatively long signals from large earthquakes, single-record estimates of H and α show significant scatter, and averaging is needed to obtain stable results.

Additional limits on bandwidth are related to our intention to obtain several independent estimates of signal parameters using a comb of HF filters with non-overlapping frequency bands. This mode of analysis pursues three aims:

1. to check the possibility that the Hurst exponent is frequency-dependent;
2. to increase the amount of independent estimates of the Hurst exponent, and thus to obtain statistically more convincing results; and, finally,
3. to analyze the largest possible number of records: with our approach, records with more narrow usable frequency range need not be excluded; they merely supply estimates for a smaller number of bands.

The structure of the paper is as follows. We begin with a short background to our processing procedures; then develop the processing algorithm and check it by applying it to simulated data with, or without, the self-similar correlated structure. Data selection and analysis are then described, first for raw data and then for less abundant deconvolved data.

2. Basics of Data Analysis

To check and verify that HF envelopes of earthquake body waves are fractal-like, we use two

techniques, both well known in this field, one in the time domain and another in the frequency domain. The time domain technique is based on the variogram (Kolmogorov–Obukhov second-order structure function or MANDELBROT's delta-variance) that is defined for the cumulative signal $Y(t)$ according to the formula:

$$V(\Delta t) = \left\langle (Y(t + \Delta t) - Y(t))^2 \right\rangle \quad (1)$$

where angular brackets denote averaging, Δt is the time lag; $Y(t)$ is integral of the analyzed stationary signal $X(t)$ reduced to zero mean:

$$Y(t) = \int (X(t) - \langle X \rangle) dt \quad (2)$$

In the processing of digitized data with a discrete time step dt , $Y(t)$ is the cumulative sum of $X(t)$, and the possible values of the lag are equal to $dt, 2dt, 3dt, \dots$. For a white noise input, $Y(t)$ is a discrete Brownian process, thus $V(\Delta t)$ behaves as a power law:

$$V(\Delta t) \approx C\Delta t^{2H} \quad (3)$$

with exponent $2H$ equal to unity. Here H is the Hurst exponent, the main parameter in a study of self-similarity. When plotted on a log–log scale, an empirical variogram of the general form given by Eq. (3) must show a linear trend with slope $2H$. For more graphical clarity, we further use a modified variogram:

$$MV(\Delta t) = V(\Delta t)/\Delta t \quad (4)$$

that must be constant for the reference case of white noise ($2H = 1$); therefore the presence of the slope of the empirical $MV(\Delta t)$ plot suggests that H differs from 0.5. In the test cases, and with real data, the slope in the relationship:

$$\log MV(\Delta t) = (2H_v - 1) \log \Delta t + b \quad (5)$$

was estimated by linear regression, here H_v is a variogram-based estimate of H .

In parallel, frequency-domain analysis was performed. For a self-similar signal, we can expect the power-law behavior for its power spectral density $PSD(f)$:

$$PSD(f) \approx C'f^\alpha \quad (6)$$

In the reference case of white noise, $\alpha = 0$; when processing real data, we are interested in an empirical estimate of α . To determine α numerically,

one can estimate $PSD(f)$ by applying the Fourier transform to the signal. Further processing is similar to that applied to the modified variogram: use linear regression for $\log(PSD)$ as a function of $\log(f)$ to estimate α , then find the estimate of H as $H_p = (\alpha - 1)/2$. In real calculations, the squared amplitude spectrum was used; this is proportional to the estimate of $PSD(f)$. The question of linearity of the relationship between $\log MV(\log \Delta t)$ and $\log PSD(\log f)$ is an important point in further analysis.

These two approaches have different strong and weak sides. Variograms behave well at small lags but become unreliable at large lags; the largest usable lag is about $0.20T$ where T is the signal duration. Adjacent points of the variogram are significantly correlated; thus the variogram is smooth, which helps in graphical analysis but may be misleading. Spectra provide unbiased estimates for frequencies as low as $f = 1/T$, but may perform worse at the uppermost frequencies. Discrete spectral ordinates are almost independent; thus empirical spectral plots look very noisy, making graphical comparison difficult. Therefore, to employ both techniques in parallel is a reasonable approach. As noted in the “[Introduction](#)”, we are forced to use narrow ranges over lag or frequency, and our individual estimates of H are rather noisy. Thus, we shall pool the data from many traces to make the results more certain.

3. Testing the Processing Procedure with Simulated Signals

Before applying our processing procedure to real data, we test it on simulated random data with known structure. Two simulated series of sample traces that represent segments of stationary noise are analyzed: the case of white noise samples with constant instant power (case WN) and the case of fractal noise (case FE). Additionally, two similar cases are simulated, with the only difference that slight modulation was added to stationary noise. In all cases, imitating a real signal of a typical BHZ channel of a GSN station, we generated discrete white noise with time step 0.05 s over the time window $T = 102.4$ s, comparable with actual durations of analyzed windows. In the WN

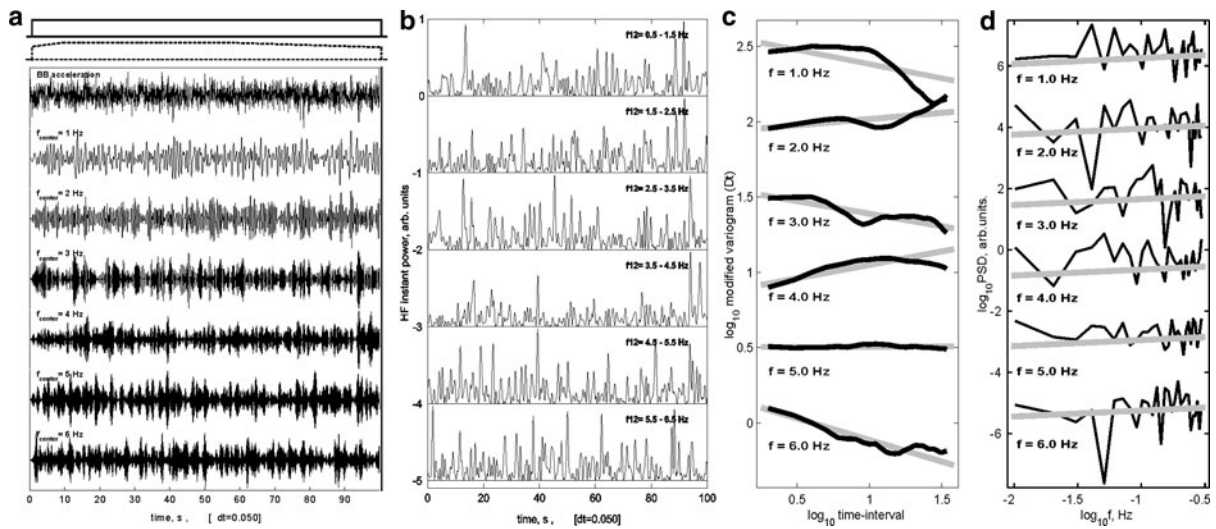


Figure 1

The processing procedure applied to a single sample function of simulated digital broadband white noise with time step 0.05 s and duration 102.4 s. **a** White noise: raw (*top trace*) and after bandpass filters; **b** Filtered signals, squared; **c** Modified variograms and their linear trends on a log–log scale; **d** PSD plots and their linear trends. In **a**, above all the signals, two variants of envelope or modulating function are shown: boxcar (*solid line*), the basic case of no modulation, producing a segment of stationary signal, processing for this case is illustrated in **b**, **c**, and **d**; and slightly rounded boxcar (*dashes*), the case subsequently used to illustrate the effects of non-stationarity

cases, this signal was used as is; in the FE cases, it was multiplied by the square root of the self-similar random envelope function. This approach was proposed by MARSAN and BEAN (2003, Sect. 2.3.3, the “derivative” or “increment” case) for the special case when the envelope function is a lognormal multifractal measure. Ideally, the output of this procedure, when squared (i.e. converted to instant power) must inherit the self-similarity of the envelope. In reality, this ideal can be approached only in two limiting cases: if signal bandwidth is much wider than the frequency range analyzed, or, equivalently, at very long periods/large lags. In both these cases the fluctuations introduced by multiplication by white noise will become negligible. In the real case, the situation is more complicated, as we shall see soon.

After simulation, the following basic processing procedure was applied. The broadband signal was filtered by a bank of bandpass filters. Six non-overlapping frequency bands are used, jointly covering the 0.5–6.5 Hz frequency range. Each filter had the same bandwidth $\Delta f = 1.0$ Hz (defined at -3 dB), and their six central frequencies were equal to 1.0, 2.0, ..., 6.0 Hz. Filtered signals are converted to an instant power estimate taken as the squared modulus

of the analytical signal (SMAS). For all bands, this operation produces smoothed output, with common correlation time of the order of $t_c = 0.5/\Delta f = 0.5$ s. Then signals are binned (smoothed-and-decimated) with the larger time step dt selected to be $2t_c = 1$ s, resulting in weakly correlated samples of instant power. Therefore, for a white-noise input, the decimated instant power signal is approximately white noise again, but with a non-zero mean.

In Fig. 1 we illustrate the WN case for a single simulated trace. In Fig. 1a, white noise signals are shown, original and filtered. On top of these, two modulating functions are shown: the boxcar that symbolizes no modulation and the slightly rounded boxcar that was used for analyzing the effect of “slow” non-stationarity. In Fig. 1b, the SMAS is given for the six bands. Figure 1c and d depict variograms and spectra on a log–log scale, together with their linear approximations. In Fig. 2, again for the WN case, stacked and averaged MV(Δt) and PSD(f) plots are given based on 100 random copies of white noise. One can see that in the analyzed ranges for lag or frequency, statistical fluctuations of individual MV(Δt) and PSD(f) functions are effectively suppressed by averaging, and approximately constant

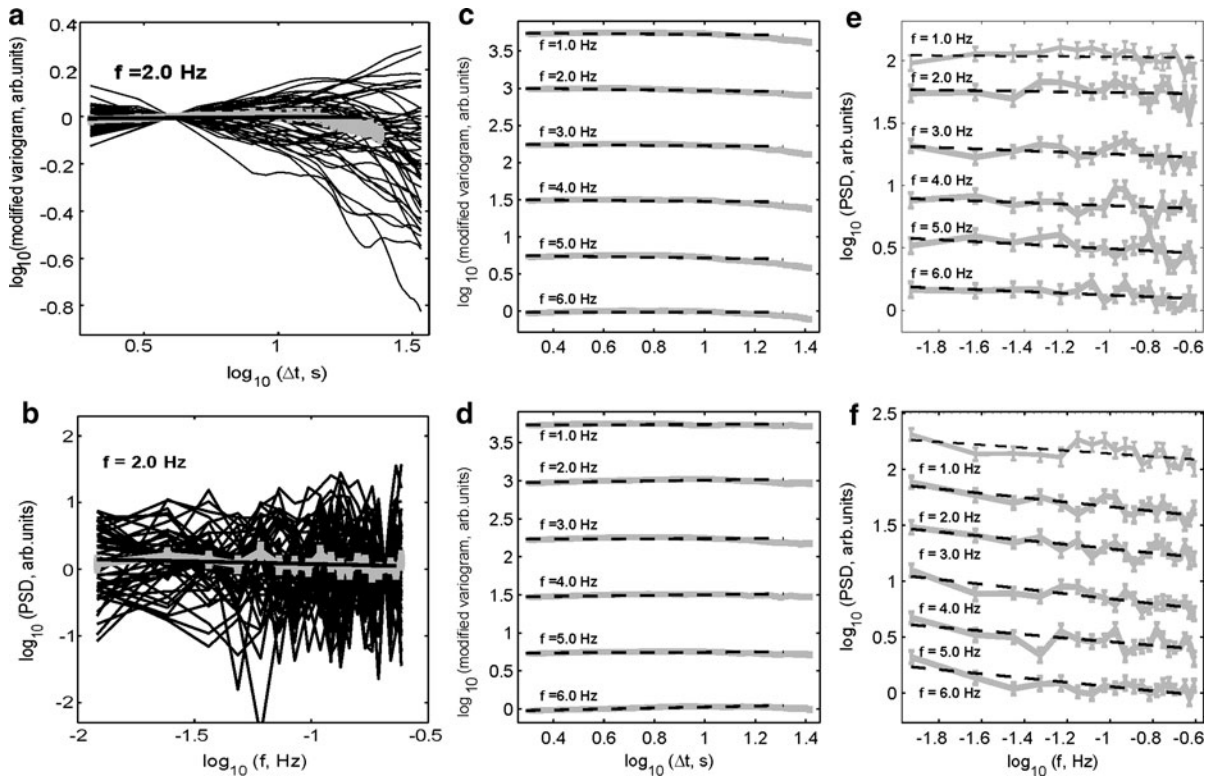


Figure 2

Average variograms and PSD plots obtained with many simulated white noise traces of the kind shown in Fig. 1. **a** 50 modified variograms of sample traces (*thin lines*) of the 2-Hz band; their average, with error bars (*grey*), and its linear approximation as the *black straight-line segment*. **b** Fifty plots of the PSD, in similar format. **c** (Modified) variograms for six bands averaged over 100 runs. **d** Similar variograms obtained with slightly non-stationary (modulated) white noise, see caption of Fig. 1a. **e** Average PSD spectra for six bands, stationary signal. **f** Similar spectra for modulated white noise. In **a** and **b**, each individual variogram and spectrum is normalized to its own value at a certain fixed lag or frequency, resulting in a bundle-like appearance. In **c**, **d**, **e** and **f**, the results for each of the six bands are similar, as expected for signals of identical bandwidth. For the stationary case, both modified variograms and spectra are approximately horizontal, as expected for the simulated delta-correlated case. For the case of the modulated noise, variograms (**d**) are visually indistinguishable from those for the stationary case (**c**); whereas the PSD spectra (**f**), are concave and decrease with frequency, the distortion produced by non-stationarity

average trends can be seen in Fig. 2c and e. The point of the variogram at $\Delta t = 1$ s is excluded, because it indicated some correlation at this lag. Above $\Delta t = 20\text{--}25$ s the linear trend of the variogram also deteriorates. Thus, the useful range of lags is limited. For PSD(f) plots, the useful frequency range is somewhat wider: it begins at $1/T = 0.01$ Hz and ends at half the Nyquist frequency, or 0.25 Hz.

Figure 2d and f illustrate the effect of “slow” non-stationarity. This effect is clearly seen for the PSD(f) plots of Fig. 2f that show generally concave shape over the entire frequency band. This distortion is concentrated at lower frequencies, and average spectral trends are near-horizontal. Such behavior matches well with that of the variogram plot, Fig. 2d,

that covers only shorter lags. Therefore, non-stationarity of the introduced kind, with long wavelength, can enhance the low-frequency part of the observed PSD(f). This kind of distortion is quite understandable and could be expected in advance. It is illustrated here mostly to provide a possibility of comparison with another cause of concavity of spectra, to be discussed soon. Still, this case reminds us that caution must be used in selecting nearly stationary segments of earthquake data.

In Fig. 3, similar plots are given for the FE case. For simulation we used the slightly modified procedure *nonconservative_III* of MARSAN and BEAN (2003), with 2,048 samples, $C_1 = 0.046$, and $\chi = 0.3$. Average MV and PSD plots, based on

stacked 200 variograms or spectra, are evidently non-constant, and show monotonous slope, as expected, showing a clear imprint of self-similarity. However, although approximately linear on a log-log scale, PSD plots bear certain systematic concavity even in the case of a stationary signal (Fig. 3d). For the non-stationary FE case (Fig. 3f), concavity is seen again, in the manner visually similar to the case of a stationary signal.

Tests were also performed using stationary traces with 131,072 points, see average MV and PSD plots in Fig. 4. It is seen that for long traces:

1. clear concavity shows itself also in the variograms, not only in the spectra, and
2. concavity of spectra is persistent and does not disappear even for rather long traces.

These facts qualitatively agree with the expected deviation of MV and PSD log-log trends from straight lines (those expected for the case of the truly self-similar signal) related to limited bandwidth. However, even with such long signals, the stable low-frequency part of spectra that can be expected for the

asymptotic case is not reached. Thus, in real cases, moderately curved, concave MV and PSD plots can be expected (and are actually observed, as we shall see soon).

It is interesting to note that to reduce limited-bandwidth-related bias in estimating slope, one would prefer to estimate the slope over the lower-frequency subrange, whereas use of the higher-frequency subrange is preferable in order to suppress the effects of non-stationarity (of the kind discussed above). Thus, one cannot reliably reduce the bias in the estimates of H simply by using the more narrow subrange of frequencies/time lags.

The slopes of the plots in Fig. 3c-f were determined by least squares over the Δt range 2–20 s for MV plots and over the $1/f$ range 4–100 s for PSD plots. The H estimates were further averaged over six bands, giving the following H estimates for the FE case: $H_v = 0.627$ and $H_p = 0.732$ for the stationary case and $H_v = 0.642$ and $H_p = 0.742$ for the non-stationary case; the rms accuracy is better than 2% in all cases. These numbers can be compared with similar estimates for the reference WN case (Fig. 2c-f)

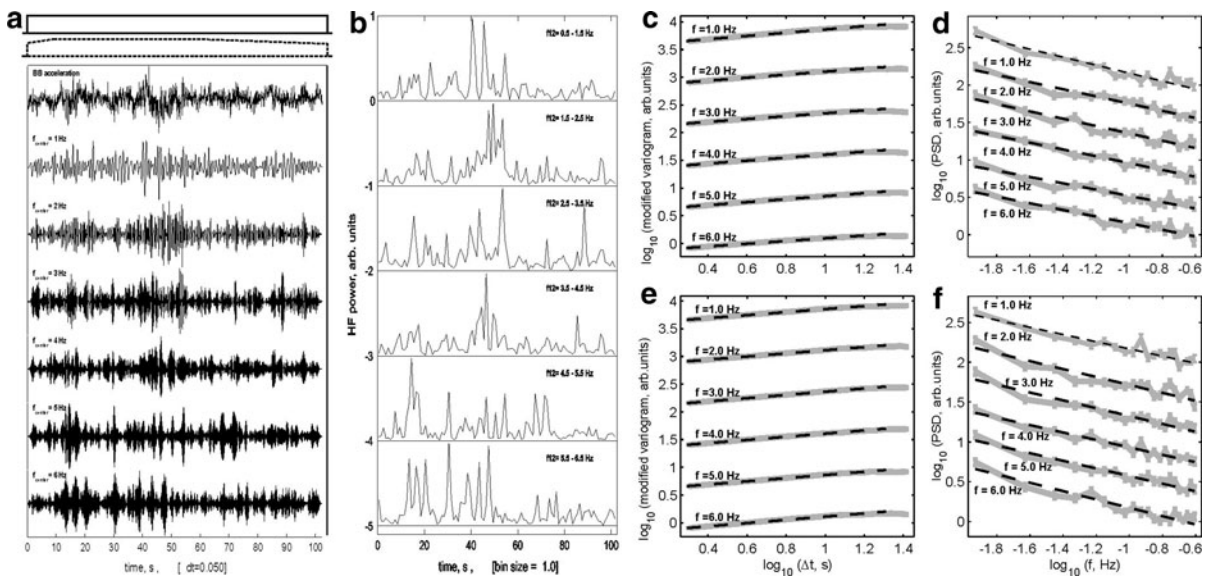


Figure 3

An example fractal-noise trace with its instant power, and average variograms and PSD plots obtained from 200 simulated traces. **a** Analog of Fig. 1a. **b** Smoothed and decimated SMAS of traces in **a** (estimated instant power), $dt = 1$ s. **c**, **d** Analogs of Fig 2c and e based on 200 variograms and spectra for the stationary case. **e**, **f** Analogs of Fig. 2d and f, again based on 200 realizations of fractal noise, but with weak non-stationarity added through the modulation function shown as the *dashed line on top of the graph a*. Note the sloped shape of the variograms and spectra, with additional slight concavity clearly seen in the spectra. In **d**, concavity is the intrinsic property of the stationary signal; in **f** also some admixture of the effect of weak non-stationarity is possible; see text for details

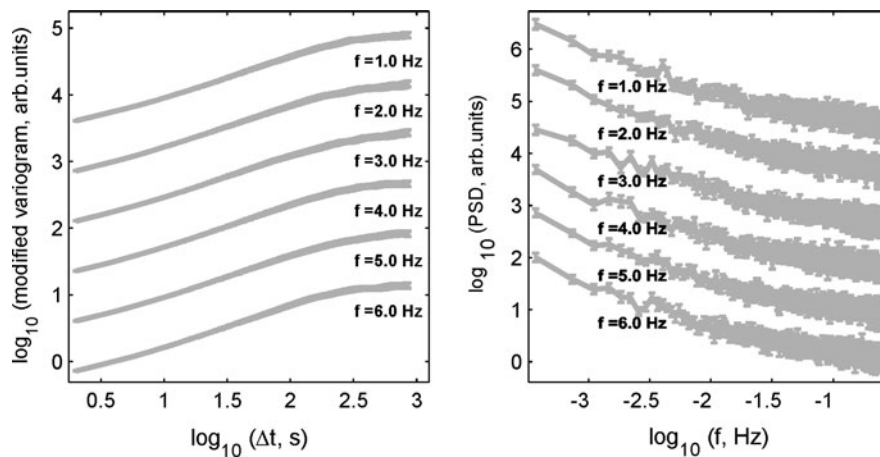


Figure 4

Analogs of Fig. 3c and d for the time window of 6,563.6 s: modified variograms on the *left*, and PSD spectra on the *right*. Stationary signals are simulated in 100 copies. Note concavity not only in the spectra but also in the variograms

that give $H_v = 0.483$ and $H_p = 0.534$ for the stationary case and $H_v = 0.514$ and $H_p = 0.592$ for the non-stationary case. These estimates bear the following information:

1. In the reference case of stationary WN a moderate mismatch is present: between H_v and H_p estimates, of the order of 0.05, and between these estimates and the true value $H = 0.5$, of the order of 0.02–0.03. This fact indicates certain bias in numerical estimates; it was considered tolerable.
2. In the same WN case, H_v estimates are much less susceptible to low-frequency modulation (increase of 0.03 compared with a twice as large increase in H_p). This difference might be expected on the basis of the fact that H_v estimates are based mainly on the higher-frequency part of the signal that is less distorted by low-frequency modulation.
3. In the stationary FE case, H_v estimates are increased by 0.15, whereas H_p values are increased by 0.21, compared with the reference case; thus, the increase for the variograms is lower. A difference of this kind follows from the same fact that H_v estimates are based mainly on the higher-frequency part of the signal; this fact introduces negative bias because the effect of limited bandwidth is most pronounced in this frequency range only. The H_p estimates must be considered as less biased by this factor.

4. In the same FE case, introducing non-stationarity has a small (statistically insignificant with 200 tries) effect on both H_v and H_p . This unexpected, useful, result means that limited non-stationarity hardly can significantly bias the estimates obtained by our procedure in the real case when the real signal is approximately fractal but some imprint of non-stationarity cannot be completely excluded.

The low-bandwidth-related concavity of the spectra (and to a lesser degree, of the variograms) that shows itself in the simulated data (and in the observed data below) deserves short discussion. First, it constitutes only a certain nonlinear perturbation of grossly linear trends of empirical variograms and spectra. Thus, its presence is not a serious difficulty for establishing the qualitative fact that observed data are far from white noise and behave in an approximately self-similar way. Such a conclusion, if certain, would be sufficiently interesting to justify the present study, and it can be tested using the estimates of H derived directly from the variograms and spectra of the empirical envelopes. These are easy to construct but, because of the discussed concavity, their numerical values depend somewhat on the selected range of lags or frequencies.

From a more general viewpoint, it may be interesting to establish (or reject) the existence of a

hypothetic self-similar modulation function (like that put in the foundation of the simulated examples above). This is a certain, not directly observable, entity; only its combination with white (or other stationary) noise is observable. If this hypothesis can be substantiated, the hypothetical modulation function would be characterized by a new “intrinsic” Hurst exponent, which depends neither on the mode of processing nor on the position of the frequency/lag window used for analysis. To verify such a model, and to estimate the value of the “intrinsic” Hurst exponent, a more advanced approach must be developed. In this paper we shall confine ourselves to the empirical H estimates only.

4. Data and examples of their processing; data segment selection

To determine H values of the HF instant power of earthquake P -wave trains, data from nine recent large earthquakes (Table 1) were used. Five events are from subduction zones, three are crustal events, and one is an outer-rise normal fault. Some of these earthquakes, and in particular their HF body waves, have been studied already. For the 2004.12.26 mega-event, Ni *et al.*, (2005), Lomax (2005) and GUSEV *et al.*, (2007) used the durations of the HF P -wave trains proper to determine source duration, orientation, length, and rupture velocity. In particular, GUSEV *et al.*, (2007) used the deconvolved source time functions of the HF instant power for many stations to reconstruct the HF spatial and temporal centroid, as described briefly in the “Introduction”. A similar study was also performed for the 2006.04.20 event (GUSEV and GUSEVA 2007) with bilateral rupture. For the 2002.11.03 event, FRANKEL (2004) reconstructed the space–time HF source structure also using envelopes of an aftershock as an empirical Green function.

The initial data used in this study were P wave records at teleseismic distances (20–100°) of the BHZ channel of GSN stations, retrieved from the IRIS DMS data center. Ten or more records were processed for each event; the average number of usable band-filtered traces was about four per record. The best records are from stations on the old continental lithosphere, for example BRVK, WRAB, FFC, ARU,

or ULN. In principle, for the objectives of this study, the original velocity record might be used; but the power spectrum of the recorded HF velocity decays rapidly with frequency. Use of such signals for analysis of envelopes causes a significant loss in information content; optimum in this respect is the spectrum that is flat within the spectral band analyzed (GUSEV *et al.*, 2007). To approach this requirement, recorded velocity is instrument and (approximately) attenuation-corrected, and converted to acceleration. The attenuation model used follows the $t^*(f)$ function of Fig. A1 of VENKATARAMAN *et al.*, (2002) with $t^*(f = 0 \text{ Hz}) = 0.9 \text{ s}$, and no distance dependence. The corrected broadband signal and the outputs of bandpass filters described above are first used to check the record quality and the signal-to-noise ratio. If the record as a whole and any of the bandpassed signals look acceptable, the analysis proper begins.

The first important step is interactive selection of the work time window. In setting the window-selection procedure, several factors were to be taken into account. First, we are interested in the analysis of the intrinsic stochastic structure of earthquake-generated signal treated as a segment of a stationary random process, thus such deterministic features as the initial speed-up and the final decay of this signal, both related to its finiteness in time, were to be excluded. Evidently, the coda, also, must be excluded. The longer the signal segment, however, the wider, on the logarithmic scale, is the lag/frequency window which can be used to derive or reject self-similarity. To check that the window is selected reasonably, one can also compare the selected window duration with the source process durations estimated by other studies. Note that the Doppler effect and the effects of fault width can modify the HF source-related duration as compared with an independent source process duration estimate.

After a few tries, the following two-step procedure was found to provide an acceptable compromise. In the first step, the preliminary wide window is set interactively, with its beginning at the first arrival (often selected using the broad-band trace) and its end deeply in the coda. This preliminary window is then narrowed automatically: its bounds are set between 5 and 85% fractions of the integral of the signal power, with integration limits defined by the

Table 1

Earthquakes analyzed, and parameters relevant to the processing of their data

yyyymmdd	M	Region/subregion/type	$N_{\text{sta}}/N_{\text{trace}}$	$2M_t$, s	S_{Dur}	T_{win}
1997.12.05	7.9	Kamchatka, Kronotsky, Su	20/78	53.2	47–63 (GUSEV and PAVLOV, 1998)	58 ± 13
1998.03.25	8.2	S. Pacific, Balleny Isles, Cr	10/26	74.8	165 (ANTOLIK <i>et al.</i> , 2000)	112 ± 30
2002.11.03	8.4	Alaska, Denali, Cr [full]	17/68	94	90 (FRANKEL, 2004)	85 ± 40
2002.11.03	8.4	Alaska, Denali, Cr [later]	17/68	94	90 (FRANKEL, 2004)	97 ± 24
2003.09.25	8.2	Hokkaido, Japan, Su	22/93	63.6	60 (YAGI, 2004)	58 ± 22
2004.12.26	9.2	Sumatra, Su	38/167	278	550 (GUSEV <i>et al.</i> , 2007)	329 ± 57
2005.03.28	8.7	Nias, Su	25/117	110	$\approx 85^{\text{a}}$	74 ± 22
2006.04.20	7.6	NE Russia, Koryakia, Cr	57/212	30.8	35 (GUSEV and GUSEVA, 2007)	36 ± 8
2006.11.15	8.1	Kuriles, Simushir, Su	16/76	100.4	112.7 (Vallée) ^b	84 ± 13
2007.01.13	8.2	Kuriles Simushir, OR	17/87	53.8	45.5+ (Vallée) ^b	64 ± 16

For the 2002.11.03 event, two variants are given: for the standard “5–85%” time window and for the hand-selected window with the first subevent excluded

N_{sta} , N_{trace} number of stations and number of filtered traces used, M_t centroid time minus origin time for Harvard CMT data, S_{Dur} estimates of HF duration or, where absent, of broadband source duration (italics), T_{win} average and standard deviation of window duration used in processing. The tectonic type of earthquake is coded: Cr, crustal; Su, subduction; OR, outer rise, normal

^a GUSEV (unpublished)

^b M. Vallée; event page at <http://www.geoazur.unice.fr>

first window. This procedure mostly follows TRIFUNAC and BRADY (1975) (“bracketed duration”, 5–95%), RAOFF *et al.*, (1999) (5–75%) and LOMAX (2005) (0–90%). In this way, the low-amplitude initial part, and the coda, are effectively cut off. In many cases, within the frames of the final 15% segment, the tail part of the source signal is quite legible. However, this tail part of the signal was cut off together with the coda; it is sacrificed in order to guarantee uniform processing with no subjective judgment. A common window is used for all bands that are regarded as usable; it is an average version over such windows for individual bands. Also, a noise window of comparable length is selected before the P arrival, and the noise power is estimated. Before determination of the $MV(\Delta t)$ and $PSD(f)$ functions, the time-averaged value of noise power is subtracted from each point of the observed signal power.

The duration estimates for individual events (average and standard deviation) obtained by the described procedure and given in Table 1 can be compared with twice the temporal centroid $2M_t$ of the seismic moment rate that accompanies the Harvard CMT solution, and also with the source process duration estimates obtained for the HF radiation, or, where it was absent, with the duration obtained by

broad-band inversion. HARA (2007) have recently shown that, on average, the HF duration and $2M_t$ match, but significant individual differences do occur. The special case is the 2002.11.03 Denali event that started as a thrust on a secondary fault and progressed as a great strike-slip event. On many records, the HF contribution of the initial subevent was dominant, making the results of the aforementioned automatic procedure doubtful. In this case, two versions of the processing were performed: with automatic window selection (code A) and with the window covering the late portion only and with the initial subevent manually skipped (code L, preferable version). In averaging over events, only the L case was included.

After selecting the data window, processing was performed as described in the previous section. The entire procedure is illustrated in Fig. 5. One can see similar steps as in Fig. 1, with added window selection and decimated power plot. In a significant proportion of the records examined, the data quality was not as good as seen in Fig. 5a, and visual checking of the data was essential. Simpler cases are those of significant microseismic noise, as in Fig. 6a. Rejection of noisy traces was performed automatically. In addition, a significant proportion of the records is generally unreliable, at least in the high-

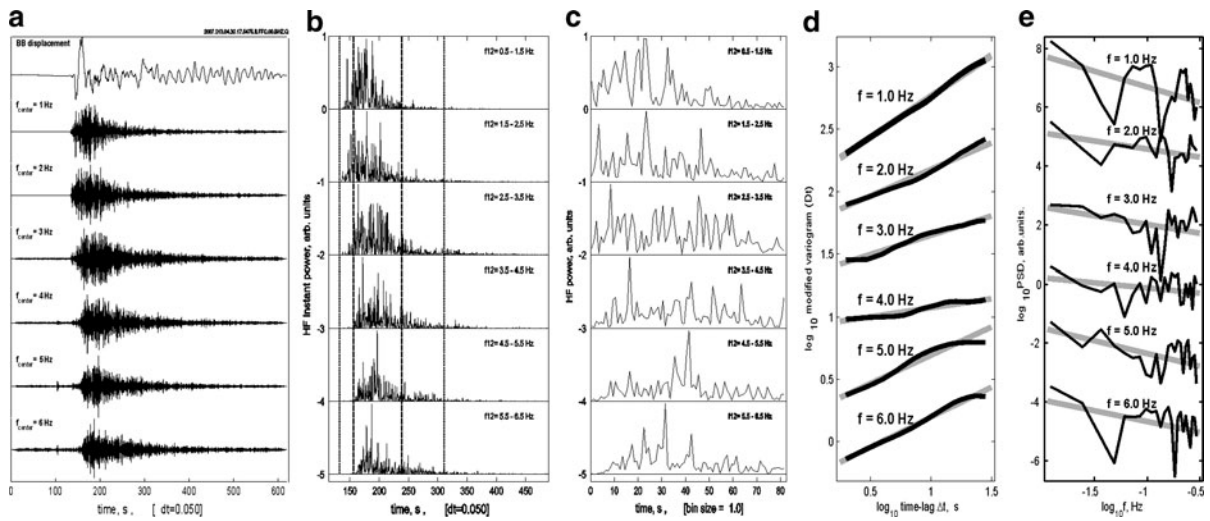


Figure 5

Processing procedure applied to the 2007.01.13 $M = 8.2$ Simushir earthquake recorded at the BHZ channel of station FFC. **a** BB displacement (*the uppermost trace*) and six filtered traces of *P*-waves. **b** SMAS (instant power) of the filtered traces of **a**; **c** Decimated smoothed power within the final window. **d** Modified variograms and, **e**, squared spectra of the window shown in **c**, with linear fit as *gray straight-line segments*; they deliver the estimates of H . In **b**, the procedure for selection of the data window is illustrated: vertical dotted lines bracket the wide hand-selected window, and vertical dashes bracket the final “5–85%” window

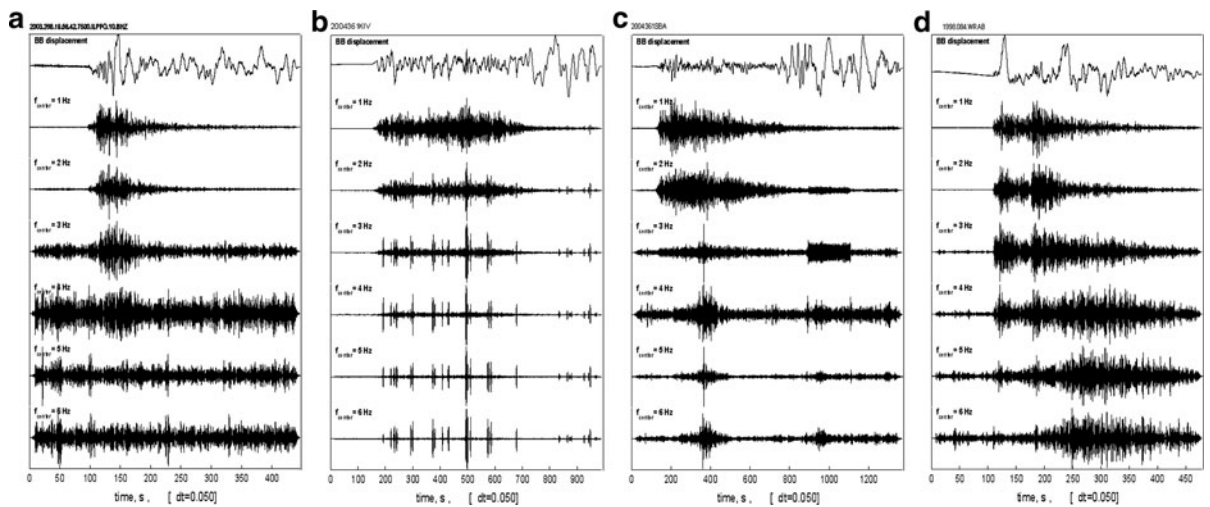


Figure 6

Examples of rejected data. **a** Event 2003.09.25 at PFO; only the two uppermost filtered traces are usable. **b** Event 2004.12.26 at KIV, spurious pulses of, presumably, instrument/digitizer origin. **c** Same event at SBA, spurious signals of unclear origin. **d** Event 1998.03.05 at WRAB. The powerful *T*-phase signal is seen above 2 Hz; only two the uppermost filtered traces are usable. Graphs are formatted as in Fig. 5a

frequency range (Fig. 6b, c). In these two and many other cases, most of spurious HF signals seem to be produced by some imperfection in the measurement channel at large amplitudes. In some cases the *T* phase overlaps the *P* group making some traces unusable (Fig. 6d).

5. Results Regarding Fractal Properties of a *P*-Wave Record

The procedure described above was applied to 239 BB records, and 992 filtered traces were found usable. For each event, the estimates of H_v and H_p were

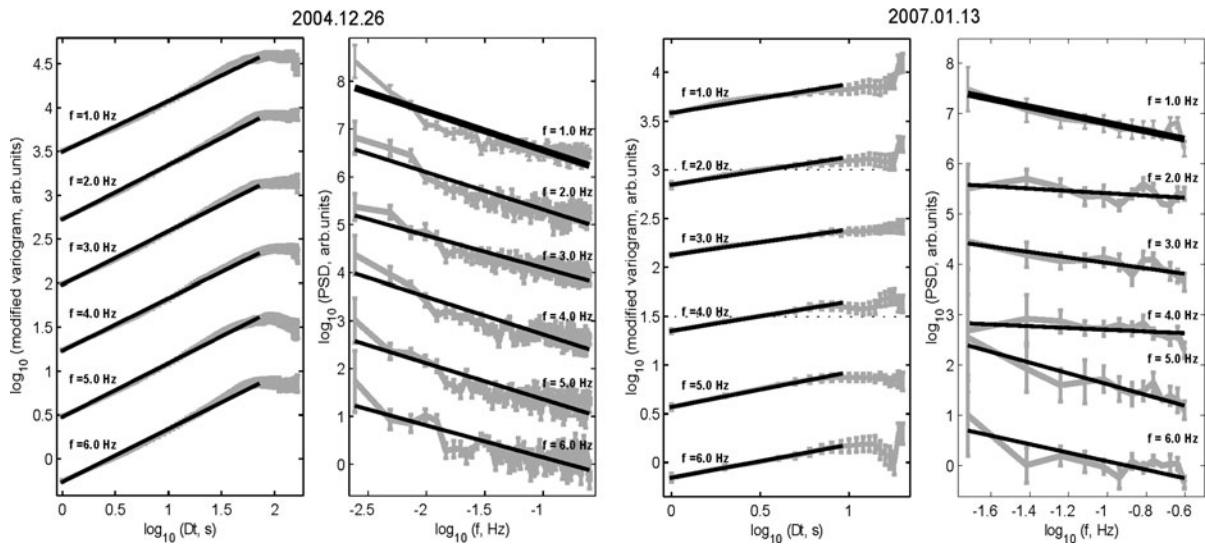


Figure 7

Average modified variograms and PSD plots obtained for the 2004.12.26 and 2007.01.13 events for six bands. Note the slight concavity noticeable for modified variograms of long records of the 2004.12.26 event

determined both individually, and from stacked variograms and PSD plots. To compensate for amplitude variation among the MV and PSD sets, each set was normalized to its own value at a fixed Δt or f (as illustrated in Fig. 2a, b). See Fig. 7 for the complete set of stacked-and-averaged variograms and spectral plots for two events, and Fig. 8 for the MV and PSD plots for the two lowermost bands with the most abundant data. Each stacked plot is based on the subset of stations contributing to this particular band. Individual graphs are dropped for graphic clarity; they would make erratic bundles similar to that shown in Fig. 2a, b. One can see that the MV and PSD plots are, generally, sloped in the same way as the MV and PSD plots for the simulated self-similar data of Fig. 3. These slopes, and the slopes of individual MV and PSD, for example Fig. 5d and e, were converted to H_v and H_p estimates that are the main indicators of self-similarity; the numerical results are given in Tables 2 and 3. One can also note that for the spectra, concavity appears quite systematically; some variograms are also clearly concave; this point is discussed later.

In Table 2, where the H_v and H_p estimates for the individual events are given with the parameters of their scatter, one can note the following.

1. All single-event estimates of H obtained by averaging of individual-trace estimates over frequency and

record are definitely above 0.5; even in the “worst” case of the 2006.04.20 event with the smallest size of data window and least accurate estimates, the rms error of the average value of $H_v = 0.56$ is about $0.15/N_{\text{trace}}^{0.5} = 0.01$; thus H_v is significantly above 0.5, and teleseismic P -wave earthquake envelopes are indeed fractal-like. All the more so for stacked-averaged H estimates for each frequency (gray lines in Figs. 7 and 8); numerically both kinds of estimates match reasonably.

2. The H_v estimates are significantly lower than the H_p estimates; the average difference is about 0.15.
3. The H_v estimates are numerically more stable than the H_p estimates, despite their more narrow logarithmic span. However, only H_p estimates should be treated as final ones, as they cover significantly (≈ 3 times) wider logarithmic span compared with the H_v estimates.
4. The inter-event component of the scatter of the H estimates, of the order of 0.06 (row 11), is significant (compare rows 11 and 12).
5. Gross averages (along the columns of Table 2, row 10) are rather stable, with accuracy of 0.02 or better (row 13).

In Table 3, of the structure similar to that of Table 2; results from alternative analyses are given, with averaging among events and records performed

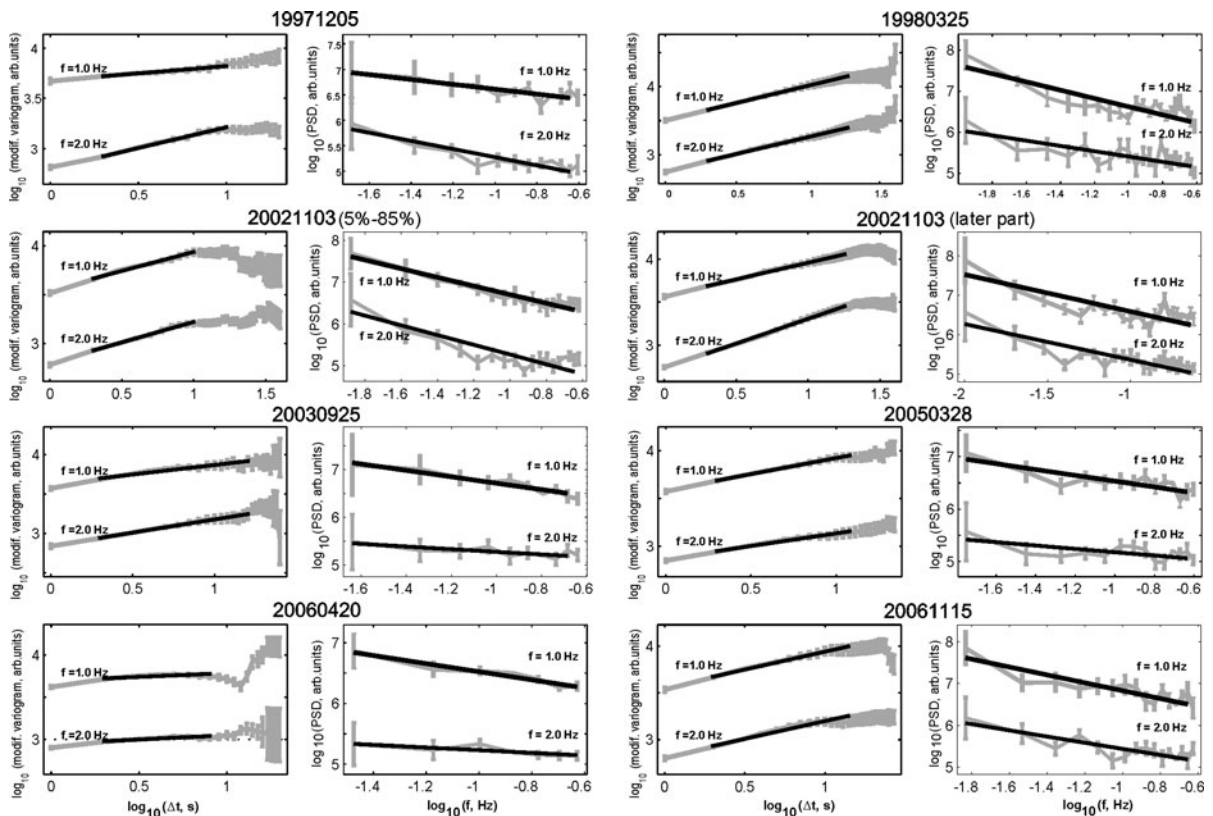


Figure 8
Average modified variograms and PSD plots obtained for the other seven events (1 and 2-Hz bands only)

separately for each frequency band. In contrast with single-event averages, single-band averages show no significant scatter (compare rows 8 and 9 that give approximately the same values). The errors for gross averages (row 10) obtained here are formal errors—see Table 2 for more realistic figures. Generally, all estimates of errors in Tables 2 and 3 are approximate. A systematic study of components of variance might be undertaken using formal tools (ANOVA), resulting in even more accurate specification of errors of the estimates, but this is hardly justified in this case. Our simple analysis shows that for the individual H_p values there are two significant components of variance—the event-related component, of the order of $(0.04\text{--}0.05)^2$, and the residual, purely random, component, of the order of 0.2^2 ; the band-related component is negligible. We did not try to study the station-related component, and considered it negligible also. For the stacked H_p estimates, the event-related component is somewhat lower but comparable, and the random component

equals 0.06^2 on average, with great scatter that does not show any relationship with the amount or quality of the data. Similar reasoning can be repeated for the stacked H_v estimates, with numerically comparable results. To summarize, we have obtained:

1. single-event H estimates, of the H_p kind, in the range 0.73–0.90, each with rms error of about 0.02; and
2. the average H over events, of the same kind, equal to 0.83, with rms error again of about 0.02; the last average depends on the small subset of events selected, and may be somewhat unstable.

The significant parameters of the scatter of the measurements are:

- single-measurement error for a certain station and a certain 1-Hz-wide band, of about 0.2, and
- inter-event fluctuations, with rms deviation of about 0.04–0.05.

Table 2

Estimates of the Hurst exponent H , for nine events, averaged over six frequency bands

No	Date	M	H_v [indiv] \pm interrecord ^a	H_v [stacked] \pm interband ^b	H_p [indiv] \pm interrecord ^c	H_p [stacked] \pm interband ^d
1	1997.12.05	7.9	0.64 \pm 0.12	0.66 \pm 0.05	0.80 \pm 0.25	0.77 \pm 0.10
2	1998.03.25	8.2	0.75 \pm 0.07	0.76 \pm 0.02	0.90 \pm 0.14	0.93 \pm 0.03
3A	2002.11.03[A]	8.4	0.75 \pm 0.10	0.78 \pm 0.03	1.00 \pm 0.25	1.02 \pm 0.08
3L	2002.11.03[L]	8.4	0.71 \pm 0.10	0.71 \pm 0.03	0.84 \pm 0.14	0.83 \pm 0.05
4	2003.09.25	8.2	0.65 \pm 0.14	0.68 \pm 0.03	0.87 \pm 0.20	0.86 \pm 0.05
5	2004.12.26	9.2	0.75 \pm 0.08	0.78 \pm 0.01	0.83 \pm 0.09	0.82 \pm 0.02
6	2005.03.28	8.7	0.65 \pm 0.13	0.68 \pm 0.03	0.82 \pm 0.19	0.80 \pm 0.07
7	2006.04.20	7.6	0.56 \pm 0.15	0.60 \pm 0.02	0.73 \pm 0.30	0.74 \pm 0.08
8	2006.11.15	8.1	0.66 \pm 0.09	0.70 \pm 0.01	0.86 \pm 0.16	0.83 \pm 0.03
9	2007.01.13	8.2	0.63 \pm 0.13	0.65 \pm 0.01	0.81 \pm 0.23	0.79 \pm 0.04
10	Average		0.67...0.11	0.69...0.025	0.83...0.19	0.82...0.058
11	St. dev		0.060	0.054	0.036	0.056
12	Error 1		0.012	0.011	0.020	0.026
13	Error 2		0.021	0.019	0.013	0.020
14	2004.12.26 [dcn]	9.2	0.64 \pm 0.13	0.69 \pm 0.07	0.89 \pm 0.21	0.86 \pm 0.16
15	2005.03.28 [dcn]	8.7	–	–	0.99 \pm 0.31	0.93 \pm 0.30

^a H_v averaged over all the individual-trace estimates and all the filtered traces; accompanied by the standard deviation among such estimates

^b H_v averaged over the six single-band estimates, each calculated from the stacked variogram for a band, accompanied by the standard deviation among the six estimates

^c H_p estimate similar to footnote a

^d H_p estimate similar to footnote b

Estimates and standard deviations of each kind are further averaged over events, making the “average” in row 10. The scatter between estimates for the individual events revealed in such averaging is given in row 11 “st. dev.”

The formal accuracy of single-event H estimates of rows 1–9 may be obtained: for the estimates labeled “[individual]” by division of the standard deviation given in each row by $N_{\text{trace}}^{0.5}$; for estimates labeled “[stacked]” H is estimated in similar way by dividing by $6^{0.5}$. Average single-event accuracy is given in row 12 “error 1”. For gross averages of row 10, accuracy can be found dividing the values of inter-event scatter in row 11 by $9^{0.5}$; the results are given in row 13 “error 2”

The line “2002.11.03[A]” is excluded from the along-column averaging. Rows 14 and 15 are similar to lines 1–9 but give results obtained from deconvolved data, with different set of bands. In the last row, no variogram-based estimates could be obtained because the log range of slope estimation was too narrow

Now let us consider the concavity of many spectral shapes and, in a less expressed form, of some of the variograms seen in Figs. 7 and 8. Looking at the data from an empirical viewpoint, one might infer from the concavity of trends that the “fractal behavior”, that is, the enhanced multi-scaled correlation as compared with the white noise, is more expressed at lags/periods comparable with entire event duration, and somewhat deteriorates at smaller lags. Such reasoning is permissible; but, as was noted in relation to the concavity of the simulated PSD plot of Fig. 3, this empirical view may be superficial. It is quite probable that at a deeper level, the entire picture is related to a modulating function with much a more perfect self-similarity pattern whereas the observed concavity is a sole effect of its combination with stationary noise of very limited bandwidth, as

explained in the previous section. At present we have no means at hand to make a definitive interpretation of the observed concavity. Despite this complication, we can claim that the bursty behavior is indeed “fractal-like”, and systematically and clearly deviates from the behavior of white noise (whose empirical envelopes do show fluctuations, but only mild ones, and are not really “bursty”).

In Fig. 9a and b one can see whether H_v and H_p are frequency-dependent. No clear variation is seen, but a slight tendency of H_p to increase with frequency can be noticed. In Fig. 9c one can see that record-averaged estimates (from MV and PSD) are correlated, as could be expected. When further averaged over frequency, these data show even more clear correlation, illustrating the mentioned notion that the inter-event variation of H is real.

Table 3

Estimates of the Hurst exponent *H* for frequency bands, averaged over nine events

No.	Frequency band, Hz	Central frequency, Hz	H_v [indiv] \pm interrecord ^a	H_v [stacked] \pm inter-event ^b	H_p [indiv] \pm interrecord ^c	H_p [stacked] \pm inter-event ^d
1	0.5–1.5	1.0	0.65 \pm 0.13	0.68 \pm 0.06	0.82 \pm 0.19	0.80 \pm 0.09
2	1.5–2.5	2.0	0.67 \pm 0.11	0.70 \pm 0.06	0.83 \pm 0.18	0.81 \pm 0.08
3	2.5–3.5	3.0	0.68 \pm 0.09	0.70 \pm 0.06	0.86 \pm 0.15	0.84 \pm 0.07
4	3.5–4.5	4.0	0.67 \pm 0.10	0.68 \pm 0.06	0.84 \pm 0.21	0.83 \pm 0.06
5	4.5–5.5	5.0	0.66 \pm 0.11	0.68 \pm 0.06	0.82 \pm 0.19	0.80 \pm 0.08
6	5.5–6.5	6.0	0.66 \pm 0.12	0.70 \pm 0.05	0.83 \pm 0.21	0.87 \pm 0.09
7	Average		0.67...0.11	0.69...0.06	0.83...0.19	0.82...0.07
8	St. dev		0.012	0.013	0.013	0.029
9	Error 1		0.012	0.021	0.020	0.025
10	Error 2		0.005	0.005	0.005	0.012
11	0.4–1.2	0.8	0.57 \pm 0.14	0.61	0.74 \pm 0.24	0.69
12	1.2–2.0	1.6	0.66 \pm 0.14	0.71	0.90 \pm 0.25	0.85
13	2.0–3.0	2.5	0.70 \pm 0.09	0.75	1.01 \pm 0.15	1.02
14	3.0–4.0	3.5	0.68 \pm 0.10	0.75	0.99 \pm 0.21	1.01

The upper part of the table is organized in the same way as Table 2, with bands replacing events and vice versa. The last four rows are for the deconvolved data of the 2004.12.26 event

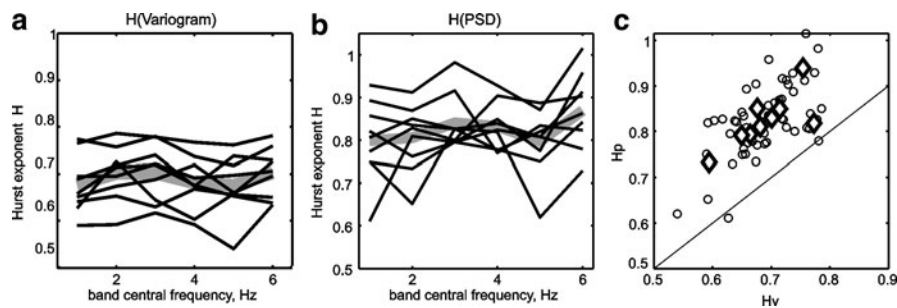


Figure 9

Variation with frequency of the estimate of *H* obtained from stacked and averaged MV and PSD. **a** $H_v(f)$ trends for each of nine events and the average trend over events (*thick gray*). **b** Similar plots for $H_p(f)$. **c** Individual H_v data points of plot **a** against the corresponding H_p points of plot **b** (*circles*); and similar representation of event-averaged $H_v(f)$ and $H_p(f)$ trends (*diamonds*)

6. Checking the Source Origin of Fractal-Like Signal

The results presented above show that the bursty behavior of the HF envelopes of the teleseismic *P*-wave records from large earthquakes is a real phenomenon with approximately self-similar signature, and that this phenomenon is not explainable by fluctuations of amplitude of the “white noise” signal. It is reasonable to attribute the cause of such behavior to a source time function, and not to a propagation effect. We already mentioned that the IPGF consists of an *P* group, commonly treated as a sequence of three delta-like spikes of *P*, *pP* and *sP* of comparable amplitude, mixed with secondary phases and followed by a

random-looking decaying tail of an *P* coda. It is almost evident that bursty envelopes cannot originate from combination of a white noise signal with a time function of this kind. However, it is interesting to show this experimentally.

Therefore we further tried to find out whether the correlation properties of envelopes, revealed above, can represent an imprint of the propagation path. In Fig. 10 one can see plots for an example of a typical moderate-magnitude event considered as an example of an EGF, namely the 2005.01.09, *M* = 6.2 aftershock of the 2004.12.26 mega-earthquake. A window length of 400 s was used. One can see that the variograms show power-law-like behavior in the rather

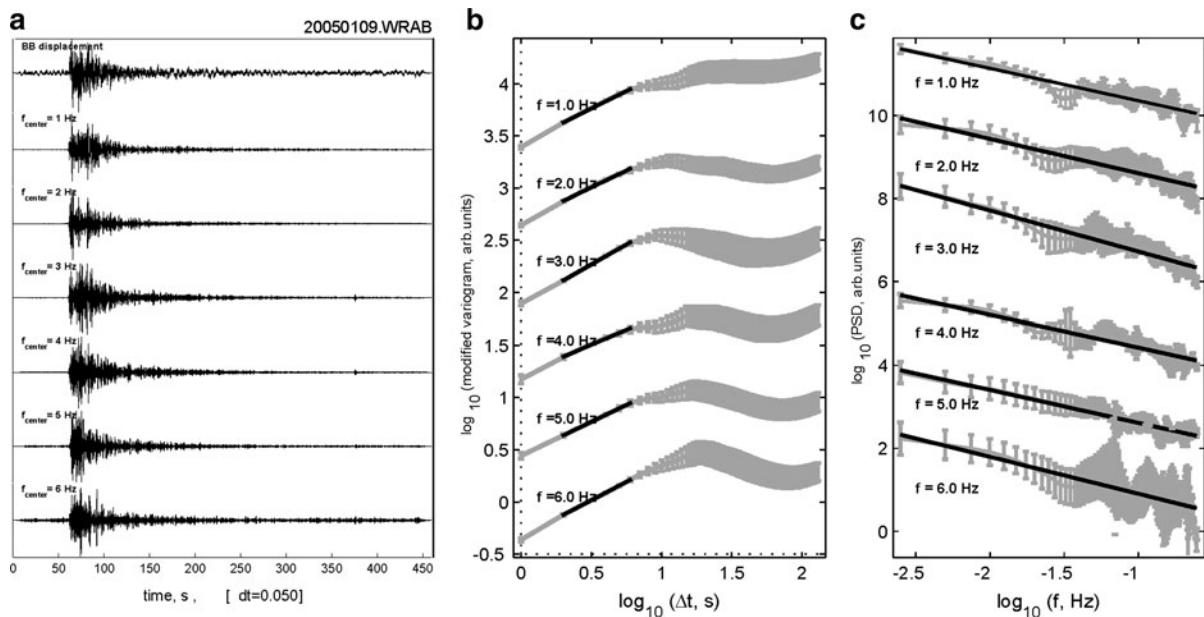


Figure 10

Example of bandpass-filtered traces of the 400-s segment of the record after the first arrival of the 2005.01.09.22.12 event ($M = 6.2$) at WRAB (a), and modified variograms (b) and spectra (c) of similar traces, averaged over 12 stations

narrow lag range 2–6 s whereas the spectral shapes are complicated. They clearly differ from the systematic uniformly decaying spectra of Figs. 7 and 8, but still somewhat resemble the power-law behavior. To clarify the situation, we studied HF instant-power source time functions with path effects stripped off by deconvolution. Data for two events were analyzed: the 2004.12.26 event, studied by GUSEV *et al.*, (2007), and the 2005.03.28 event. The processing procedure derived above was now applied to deconvolved source time functions; the only difference was that time window limits were adjusted to sufficiently well-defined moments of the beginning and the end of the deconvolved pulse. The deconvolution (inverse filtering) of path effects had been applied to the SMAS of the band-filtered P -wave signal averaged over the 10-s window (5-s window for the 2005.03.28 event). The set of four bands was used, namely 0.4–1.2, 1.2–2, 2–3, and 3–4 Hz. As an empirical Green function for a particular source-to-station path, the record of the 2005.02.26.12.59 aftershock of the 2004.12.26 event obtained by the same station was used, for both 2004.12.26 and 2005.03.28 events (both epicentral areas are located nearby and abut one another). In

Fig. 11, one can see an example of a deconvolved time function, and the average MF and PSD plots obtained for the 2004.12.26 event using 38 stations (of these 38 cases, in 12 cases, the EGF was constructed from the record of the station KURK instead of the record of the same station). For the 2005.03.28 event, 26 stations were used. Note that the deconvolved pulse of Fig. 11a is visually quite bursty; tens of examples of such pulses for various stations can be seen in Fig. 6 of GUSEV *et al.*, (2007). In the MV trend estimation, the smallest Δt of 10 s (or 5 s) was discarded again because of noticeable artificial correlation of adjacent points of the deconvolved signal (introduced by slight smoothing within the inversion procedure). The results of processing for the 2004.12.26 event (Table 2, last but one row) were qualitatively similar and numerically comparable with those obtained in the analysis of the same event using raw wavetrains. An interesting feature is the rather clear and statistically significant increase of H with frequency, as can be seen in Table 3, and as is evident in Fig. 11. For the 2005.03.28 event, of duration about 85 s, the log ranges for frequency and, especially, for lag were very narrow. As a result, it

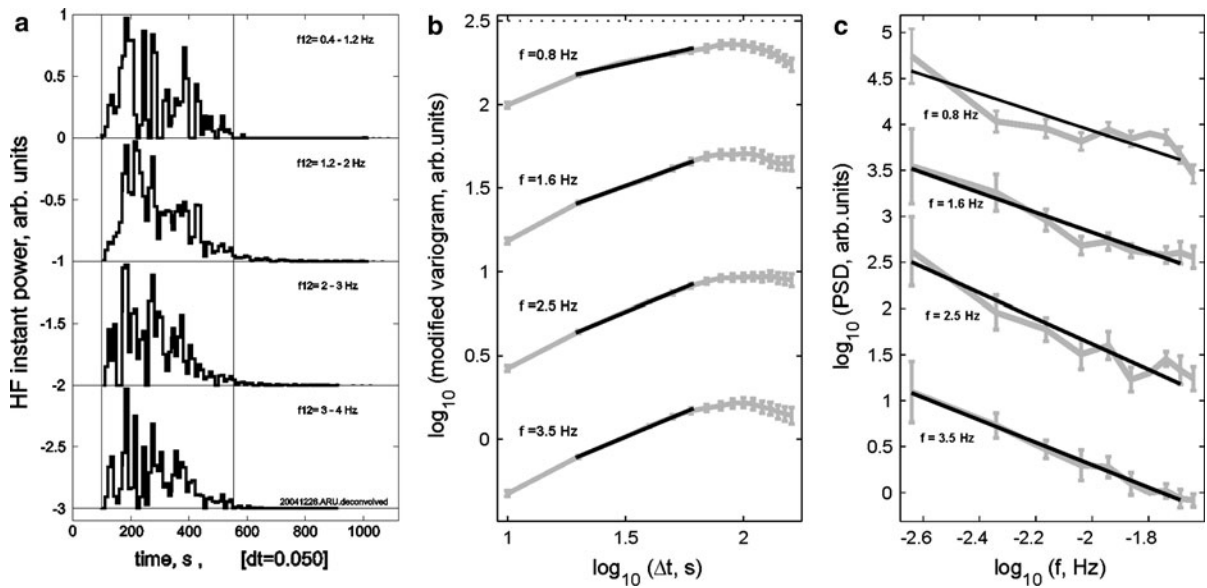


Figure 11

Example of reconstructed source instant power signal radiated by the 2004.12.26 event in the direction of station ARU for four frequency bands (a); and modified variograms (b) and spectra (c) of similar traces, averaged over 38 stations

was impossible to estimate H_v . The H_p estimates are noisy but numerically they are all about 0.95–1.0; thus they support again our assumption of $H > 0.5$.

It is interesting to compare the estimates of H obtained from:

1. the variograms;
2. the spectra of the raw records; and
3. the spectra of deconvolved signals.

These three modes are listed in order of increasing central value of the lag or period. One can see that corresponding estimates in Table 2 are ever increasing: about 0.76, 0.82, and 0.88. Of course, this is one more confirmation of the aforementioned concavity; but from another viewpoint this tendency suggests that the “ideal” estimates of H_p , in the practically unattainable limit of very long windows, may approach 1.0. Another remarkable point is that the spectra for the deconvolved data do not show concavity. This is reasonable, because each point of the deconvolved time history is a linear combination of many tens of points of the raw filtered instant power function and thus is statistically much more stable; this is equivalent to a significant increase of (relative) bandwidth.

Concluding the section, we can note that, after compensation for the propagation effect, the fractal-

like behavior of the time functions is completely preserved in all the cases analyzed, giving solid support to our idea that the fractal-like behavior is a feature of the source signal.

7. Discussion

We have shown with some confidence that the bursty behavior of envelopes of teleseismic HF *P*-wavetrains has a fractal-like signature both in the time domain and in the frequency domain. By analysis of the deconvolved envelopes, we have also shown that this behavior can be definitely attributed to the properties of the source time function (as formed in the direction of the ray to the recording station). Although this second statement is based on a smaller amount of data, and on narrower log spans of time lag and frequency, it still seems reliable. What follows from this result for earthquake fault physics?

One can believe that analysis of the correlation structure of temporal organization of fault-radiated HF energy can elucidate the organization and properties of rupture formation. It is common to treat the propagating earthquake rupture in the framework of the concept of a growing shear crack, using such

notions as fault-average stress drop, cohesion zone width, etc. In such treatment, only two characteristic times/frequencies typically appear, one related to crack size and another to cohesion zone width. One more characteristic time is the rise time, or slip pulse duration (HASKELL 1966; HEATON 1990), but it is somewhat alien to the crack concept. However, the dynamics of a real rupture have, rather, a multiplicity of scales. This property manifests itself most clearly in the now classical omega-squared source spectrum models of AKI (1967) that predict random/stochastic HF radiation with power law (i.e. self-similar) spectral shapes at frequencies significantly above the corner frequency. (The omega-squared model of BRUNE (1970) is intrinsically deterministic, but is commonly used as a stochastic model also.) However, this model says nothing about the structure of envelopes; also, real spectra deviate significantly from this model and show non-scaling spectral shapes (GUSEV, 1983). A purely kinematic stochastic self-similar space-time fault model with multi-scaled properties was proposed by ANDREWS (1981). However, with regard to the time structure of HF record envelopes, this model assumes, in essence, a simple deterministic envelope structure. Another well known broad-band fault description is the specific barrier model of PAPAGEORGIOU and AKI (1983). No manifestation was found here of characteristic subcrack duration that can be expected on its basis.

The approximately self-similar behavior of band-passed wave power revealed above gives direct support to the idea that there is a multiplicity of temporal scales in the earthquake fault process. Also, there must be a specific relationship between adjacent scales that reproduces itself from scale to scale, making the entire process self-similar. ANDREWS (1978) proposed such a hierarchical relationship for seismicity; here it is assumed for a single event. Note that there is no need to relate each scale to a population of individual sub-events of a specific size and/or duration, as was hypothesized by BLANDFORD (1975) or HANKS (1979). The discussed concept of multiplicity of scales in an earthquake rupture has not much in common with the traditional view of brittle crack with only two widely separated scales, as mentioned above.

The relationship between our results and the model of band-limited white noise proposed for HF

(acceleration) body wave earthquake signals by McGUIRE and HANKS (1981) and BOORE (1983) should be clarified. These models use deterministic and smooth or constant envelope functions, and the associated value of the Hurst parameter H must be equal to 0.5, in contrast with the estimates obtained above. Figures 1 and 2 illustrate this point. (Signals plotted there are of relatively narrow bandwidth compared with the bandwidth of an accelerogram; but this difference is not relevant.). The model discussed here is different: envelopes are not smooth functions, or deterministic functions at all; they are random. Note that the models of HANKS and McGUIRE (1981) or BOORE (1983) are correctly called “stochastic”, but one need not limit the use of this term by applying it only to the noise with constant or smoothly varying mean instant power. More general stochastic models of the HF radiation signal are possible; the one considered here, with random mean instant power, may be called “doubly stochastic” by analogy with the well-known Cox or compound point process that is a Poisson process with randomly fluctuating point rate. As another illuminating and closer analogy one can mention such concepts of modern financial mathematics as heteroscedastic Gaussian white noise with time-varying variance, or “volatility clustering”.

Phenomenologically, partly drawing from the technique of MARSAN and BEAN (2003), one can approximately treat the high-frequency body wave radiation from an earthquake source as a product of three time functions:

1. stationary random noise (band-limited, white, or colored, with constant ensemble mean variance);
2. the square root of a stationary random positive envelope function with a power-law spectrum; and
3. a boxcar or tapered (e.g., trapezoidal) window function that cuts out the finite-duration signal.

Note that there is a confusing terminological difficulty here. Let us consider a simple case of an envelope function obtained from band-limited positive white noise (say, with Raleigh-distributed samples) by fractional integration, i.e., by multiplication by $1/f^{\alpha/2}$ in the frequency domain. In mathematical terminology, such a random function with its power-law ($1/f^{\alpha}$) spectrum, is, at $\alpha < 1$,

“technically” stationary. This usage evidently disagrees with geophysicists’ intuition, because such a function has Fourier components whose amplitudes diverge as f approaches 0. The mathematician’s view is based on the fact that the power spectrum of such a signal is integrable in the vicinity of zero; for a geophysicist, however, it is unnatural to call stationary a function that contains long period components of ever-growing scale (the longer the period, the larger the amplitude). Therefore, we come to a quandary: to call real earthquake envelopes or their models, for example Fig. 3, stationary is technically correct but counterintuitive; to call them non-stationary is intuitive but formally incorrect.

One might describe the class of functions in question, formally stationary but with spectral density divergent at zero frequency, as “intermittent-stationary”. Then, we could state that the HF body waves have (approximately) intermittent-stationary random envelopes, and are (approximately) intermittent-stationary themselves. Of course, this can be said only about the middle part of the finite-duration window. The discussed representation of the body-wave signal as a product of three functions has actually been used to create test signals similar to those shown in Fig. 3. This technique can be immediately used for simulation of HF body waves from earthquakes.

It is interesting to note that apparently similar concavity of power spectra and, less clearly, variograms was found both in real data and in simulated signals of correlated noise. This finding suggests that this concavity is likely to be a secondary effect and that the underlying process is a self-similar one. However, a possibility cannot be excluded that the observed concavity is a complex phenomenon, with admixture of real deviations of the source from accurate self-similarity. Study of this problem is left for the future.

The results obtained provide an important constraint for the development of realistic broad-band models of earthquake rupture formation. They also provide a useful check for validation of simulation codes aimed at realistic imitation of strong ground motion: a reliable model must generate far-field HF radiation with realistic spectra of instant power.

8. Conclusions

1. Analysis of variograms and power spectra of envelopes of teleseismic high-frequency P waves of nine large ($M = 7.6\text{--}9.2$) earthquakes, performed in parallel in six non-overlapping frequency bands, have shown that the time functions of the envelopes, that show up as bursty and intermittent, are approximately self-similar, as reflected in approximately power-law shapes of the variograms and spectra. The related estimates of the Hurst exponent H are mostly in the range 0.6–0.9. No clear frequency dependence of H is found.
2. In the second approximation, average spectra, when plotted on a log–log scale, are in many cases moderately concave. Some variograms, with wider log span, are also slightly concave. Similar concavity was also found in simulated signals with intermittent envelopes. A simple explanation of this concavity is that it is a biasing effect of limited bandwidth; with the underlying process quite self-similar. Still, real deviations from accurate self-similarity are also possible as an additional factor. As a result of this concavity, the estimates of H obtained from variograms and spectra are systematically different (because non-equivalent ranges of periods/lags are used). The most reliable gross average estimate of H , obtained from spectra, is 0.83; but this may include bias related to the described complications. The true value of H may be somewhat larger. Inter-event standard deviation of estimates of H is about 0.05, probably reflecting the slight individual variation of H among earthquakes.
3. The developed approach was also applied to recovered pulses of HF power radiated by the 2004.12.26 mega-earthquake, with signal distortions caused by path effects stripped off by deconvolution (pulses reduced to the source). Both for variograms and spectra, the power-law behavior of the described kind was preserved, indicating that the observed approximate self-similarity of teleseismic P wavetrains is of source origin and does not represent an imprint of propagation path.

4. One can believe that the nearly self-similar correlation structure of the instant power time functions of HF waves reflect similar properties of the propagating earthquake rupture. This suggests that the earthquake rupture process is multiscaled, with fractal features, and cannot be reduced to smooth brittle crack propagation, with only two separate characteristic scales.
5. To imitate approximately HF body wave trains in practice, they may be represented as a product of three time functions: stationary colored noise with appropriate spectral shape, stationary (“intermittent-stationary”) random self-similar envelope function, and, to construct signal with appropriate duration, a boxcar or another simple window.
6. The approximate self-similarity of HF wave envelopes is their important phenomenological property. One can use this to verify how realistic are the simulated earthquake source functions used for synthesis of ground motions for engineering applications.

Acknowledgments

The study was supported by the Russian Foundation for Basic Research (Grant No 07-05-00775). Valuable comments of anonymous reviewers helped to improve the paper.

REFERENCES

- AKI, K. (1967), *Scaling law of seismic spectrum*, J. Geophys. Res. 72, 1217–1231.
- ANDREWS, D. J. (1978), *Coupling of energy between tectonic processes and earthquakes*, J. Geophys. Res. 83, 2259–2264.
- ANDREWS, D. J. (1980), *A stochastic fault model. 1. Static Case*, J. Geophys. Res. 78, 3867–3877.
- ANDREWS, D. J. (1981), *A stochastic fault model. 2. Time-dependent case*, J. Geophys. Res. 86, 10821–10834.
- ANTOLIK, M., KAVERINA, A., and DREGER, D. (2000), *Compound rupture of the great 1998 Antarctic Plate earthquake*, J. Geophys. Res. 105, 23825–23838.
- BLANDFORD, R. R. (1975), *A source theory for complex earthquakes*, Bull. Seismol. Soc. Am. 65, 1385–1405.
- BOORE, D. M. (1983), *Stochastic simulation of high-frequency ground motions based on seismological models of the radiated spectra*, Bull. Seismol. Soc. Am. 73, 1865–1894.
- BRUNE, J. N. (1970), *Tectonic stress and the spectra of seismic shear waves from earthquakes*, J. Geophys. Res. 75, 4997–5009.
- FRANKEL, A. (2004), *Rupture process of the M 7.9 Denali Fault, Alaska, Earthquake: subevents, directivity, and scaling of high-frequency ground motions*, Bull. Seismol. Soc. Am. 94, S234–S255.
- GUSEV, A. A. (1983), *Descriptive statistical model of earthquake source radiation and its application to an estimation of short-period strong motion*, Geophys. J. R. Astron. Soc. 74, 787–808.
- GUSEV, A. A. and PAVLOV, V. M. (1991), *Deconvolution of squared velocity waveform as applied to study of non-coherent short-period radiator in earthquake source*, Pure Appl. Geophys. 136, 235–244.
- GUSEV, A. A. and PAVLOV, V. M. (1998), *Preliminary determination of parameters of the high-frequency source for the Dec 05, 1997 $M_w = 7.9$ Kronotsky earthquake*, XXVI Gen. Assembly, Eur. Seismol. Commission, Papers, Tel-Aviv, Israel, 73–77.
- GUSEV, A. A., GUSEVA, E. M., and PANZA, G. F. (2007), *Size and duration of the high-frequency radiator in the source of the 2004 December 26 Sumatra earthquake*, Geophys. J. Int. 170, 1119–1128. doi:10.1111/j.1365-246X.2007.03368.x.
- GUSEV, A. A. and GUSEVA, E. M. Preliminary estimation of parameters high-frequency source of 2006.04.2006 Olyutorsky earthquake ($M_w = 7.6$, Koryuakia). In: Olyutorskoye zemletryasenie 20(21) aprelya 2006 g, Koryakskoye nagorye. Pervye rezultaty issledovaniy (ed CHEBROV, V. N.) (GS PAN, Petro-pavlovsk-Kamchatskiy, 231–240, 2007).
- HANKS, T. C. (1979), *b Values and ω - γ seismic source models: implications for tectonic stress variations along active crustal fault zones and the estimation of high-frequency strong ground motion*, J. Geophys. Res. 84, 2235–2242.
- HANKS, T. C. and MCGUIRE, R. K. (1981), *The character of high-frequency strong ground motion*, Bull. Seism. Soc. Am. 71, 2071–2095.
- HARA, T. (2007), *Measurement of the duration of high-frequency energy radiation and its application to determination of the magnitudes of large shallow earthquakes*, Earth Planets Space 59, 227–231.
- HASKELL, N. A. (1966), *Total energy and energy spectral density of elastic wave radiation from propagating faults. II. A stochastic fault model*, Bull. Seism. Soc. Am. 56, 125–140.
- HEATON, T. H. (1990), *Evidence for and implications of self-healing pulses of slip in earthquake rupture*, Phys. Earth Planet. Inter. 64, 1–20.
- HOUSTON, H. and KANAMORI, H. (1986), *Source spectra of great earthquakes: teleseismic constraints on rupture process and strong motion*, Bull. Seism. Soc. Am., 76, 19–42.
- IZUTANI, Y. and HIRASAWA, T. (1987), *Use of strong motion duration for rapid evaluation of fault parameters*, J. Phys. Earth 35, 171–190.
- KOPNICHIEV, YU. F. (1977), *A method for determination of the structure of radiation of a strong earthquake from envelope shape of P wave*, Dokl. Acad. Sci. USSR 234,794–797 (in Russian)
- Lomax, A., (2005), *Rapid estimation of rupture extent for large earthquakes: application to the 2004, M9 Sumatra-Andaman mega-thrust*, Geophys. Res. Lett. 32, L10314. doi:10.1029/2005GL022437.
- MANDELBROT, B. B. *The Fractal Geometry of Nature* (W.H. Freeman, New York 1982).
- MARSAN, D. and BEAN, C. J., *Multifractal modeling and analyses of crustal heterogeneity. In Heterogeneity in the Crust and Upper Mantle: Nature, Scaling, and Seismic Properties* (eds. GOFF, J. A.

- and HOLLIGER, K.) (Kluwer Academic/Plenum Publishers, 207–236, 2003).
- NI, S., KANAMORI, H., and HELMBERGER, D. (2005), *Energy radiation from the Sumatra earthquake*, Nature 434, 582
- PAPAGEORGIOU, A. S. and AKI, K. (1983), *A specific barrier model for the quantitative description of inhomogeneous faulting and the prediction of the strong ground motion. I. Description of the model*, Bull. Seism. Soc. Am. 73, 693–722.
- RAOOF, M., HERMANN, R. B., and MALAGNINI, L. (1999), *Attenuation and excitation of three-component ground motion in Southern California*, Bull. Seism. Soc. Am. 89, 888–902.
- RYKUNOV, L. N., SMIRNOV, V. B., STAROVOYT, YU. O., and CHUBAROVA, O. S. (1987), *Temporal self-similarity of seismic emission*, Dokl. Acad. Sci. USSR 297, 1337–1341 (in Russian)
- TRIFUNAC, M. D. and BRADY, A. G. (1975), *A study on the duration of strong earthquake ground motion*, Bull. Seism. Soc. Am. 65, 581–626.
- URQUIZU, M. and CORREIG, A. M. (1998), *Analysis of seismic dynamical systems*, J. Seismol. 2, 159–171
- VENKATARAMAN, A., RIVERA, L., and KANAMORI, H. (2002), *Radiated energy from the 16 October 1999 Set Hector Mine earthquake: regional and teleseismic estimates*. Bull. Seismol. Soc. Am. 92, 1256–1265. doi:[10.1785/0120000929](https://doi.org/10.1785/0120000929)
- Yagi, Y. (2004), *Source rupture process of the 2003 Tokachi-oki earthquake determined by joint inversion of teleseismic body wave and strong ground motion data*. Earth Planets Space 56, 311–316

(Received December 21, 2008, revised December 14, 2009, accepted January 14, 2010, Published online March 16, 2010)